Key Issues in Decomposing FMRI during Naturalistic and Continuous Music Experience with Independent Component Analysis

Fengyu Cong[1], Tuomas Puoliväli[1], Vinoo Alluri[1,2], Tuomo Sipola[1], Iballa Burunat[1,2], Petri Toiviainen[2], Asoke K. Nandi[3,1], Elvira Brattico[2,4], Tapani Ristaniemi[1]

1. Department of Mathematical Information Technology, University of Jyväskylä, Finland
2. Finnish Centre of Excellence in Interdisciplinary Music Research, University of Jyväskylä, Finland
3. Department of Electronic and Computer Engineering, Brunel University, UK
4. Cognitive Brain Research Unit, Institute of Behavioral Sciences, University of Helsinki, Finland

Corresponding author:

Fengyu Cong

Address: Department of Mathematical Information Technology, PL 35 (Agora), University of Jyväskylä, 40014, Jyväskylä, Finland

Tel.: +358-40-8053255

Fax: +358-14-2604981

Email: Fengyu.Cong@jyu.fi, FengyuCong@gmail.com

Abstract

Background

Independent component analysis (ICA) has been often used to decompose fMRI data mostly for the resting-state, block and event-related designs due to its outstanding advantage. For fMRI data during free-listening experiences, only a few studies applied ICA.

New Method

For processing the fMRI data elicited by 512-second modern tango, a FFT based band-pass filter was used to further pre-process the fMRI data to remove sources of no interest and noise. Then, a fast model order selection method was applied to estimate the number of sources. Next, both individual ICA and group ICA were performed. Subsequently, ICA components whose temporal courses were significantly correlated with the acoustical features of music were selected. Finally, for individual ICA, common components across majority of participants were found by diffusion map and spectral clustering.

Results

The extracted spatial maps (which were common across most participants, and within and surrounding the auditory cortices and slightly right-lateralized) by the new ICA approach were found relevant to the features of music.

Comparison with Existing Method(s)

Compared with the conventional ICA approach, more participants were found to have the common spatial maps extracted by the new ICA approach. Conventional model order selection methods underestimated the true number of sources in the conventionally pre-processed fMRI data for the individual ICA.

Conclusions

The further pre-processing by a reasonable band-pass digital filter can greatly benefit the following model order selection and ICA on fMRI data during real-world experiences. Diffusion map and spectral clustering are straightforward to find common ICA spatial maps.

1. Introduction

In the past twenty years, there has been a growing interest in the study of functional magnetic resonance imaging (fMRI) (Pan et al., 2011). With fMRI, a new window is opened to study cognitive brain function of human beings in processing speech, music, emotion, pictures and so on, independently and interactively (Hickok et al., 2003,Koelsch., 2010,Price., 2010,Tootell et al., 1998,Koelsch et al., 2005). Conventionally, paradigms to actively elicit fMRI data include the block design and the event-related design (Pan et al., 2011). For the block design, the contrast of fMRI data between the stimulus onset and the stimulus offset is analyzed. For the event-related one, the design matrix can be used for regression during which the temporal course of a voxel and the corresponding spatial map are learned. With the development of fMRI research, some studies even reported the fMRI data in the real experience environment where the stimulus is naturalistic, continuous and long (Alluri et al., 2012,Hasson et al., 2004,Haynes and Rees., 2006,Kauppi et al., 2010,Kay et al., 2008,Spiers and Maguire., 2007). Such naturalistic brain data can provide much richer brain responses for research. However, it tends to be difficult to obtain the contrast or the design matrix according to the experimental design. Hence, the data driven data processing methods, like independent component analysis (ICA) can be one candidate to process the challenging data (Malinen et al., 2007,Ylipaavalniemi et al., 2009).

Since 1998 (McKeown et al., 1998) ICA has been extensively used for the fMRI data processing. For different definitions of samples and variables in the linear transform model, the application of ICA can be divided into temporal ICA and spatial ICA (McKeown et al., 1998,Erhardt et al., 2010,Calhoun et al., 2001,Hu et al., 2005,Lee et al., 2010). In the former, an independent component is a temporal course. For the latter, an independent component is a voxel series which can be assembled into a spatial map of fMRI. Given the typical dimensions of fMRI datasets, the spatial ICA is usually preferred both for the plausibility of the underlying neurophysiological model and for computational requirements. Hence, the spatial ICA is chosen for the fMRI data analysis in this study. Hereinafter, when ICA is mentioned, it is referred to spatial ICA.

ICA can be further divided into individual ICA for an individual dataset (e.g., including one participant's data) and group ICA for the concatenated dataset (e.g., including multiple participants' data) (Calhoun et al., 2009). Group ICA can be even categorized the temporal concatenation approach (e.g., multiple participants' data are concatenated in the time domain) and the spatial one (e.g., multiple participants' data are concatenated in the spatial domain) (Calhoun et al., 2009). The temporal and spatial approaches allow examining individual temporal courses and individual spatial maps, respectively, and they provide common spatial maps and common temporal courses over multiple participants, respectively. Actually, group ICA requires additional assumptions besides those needed by individual ICA (Cong et al., 2013). It is unknown whether fMRI data during real-world experiences can meet the additional assumptions. Consequently, both individual ICA and group ICA are applied to decompose the fMRI data here to examine whether similar findings can be obtained by both methods.

No matter which means of ICA is applied, it is very critical to determine the number of extracted components. Model order selection (MOS) has been applied for this purpose (Li et al., 2007) and the information theory based MOS algorithms are often used, for example, Akaike's information criterion (AIC) (Akaike., 1974), Minimum Distance Length (MDL) (Rissanen., 1978), and Kullback-Leibler information criterion (KIC) (Cavanaugh., 1999). This type of MOS algorithms assumes the data are independently and identically distributed and the collected brain data have to be resampled to satisfy this assumption for MOS (Li et al., 2007). In this study, we examine another recently developed algorithm called SORTE (He et al., 2010) for MOS of fMRI data. SORTE is very efficient in the computing and does not require the resampling process (He et al., 2010). Although MOS has been extensively used for fMRI data, there are few explicit methods to validate whether the estimation of MOS is accurate or not for the real fMRI data. Recently, a simulation study has shown that MOS cannot precisely estimate the number of sources in the linear transform model when signal-noise-ratio (SNR) is low (e.g., less than 0

dB), and that when SNR is low SORTE and MDL tend to overestimate and underestimate the true number of sources, respectively (Cong et al., 2012). In this study, SORTE, AIC, MDL and KIC are performed on the conventionally preprocessed fMRI data and further preprocessed (by a digital filter) fMRI data to examine their performance in estimating the number of sources in fMRI data of individual participants.

For individual ICA, clustering the extracted ICA components of fMRI data is usually applied to find the common components across different participants, and the similarity matrix based hierarchical clustering has been often used (Calhoun et al., 2009,Esposito et al., 2005). The number of ICA components (n) is always much smaller than the number of voxels (p). In fMRI data, p can be hundreds of thousands. For the very high-dimensional data, dimension reduction tends to be performed before machine learning, like clustering and classification. In this study, a recently developed dimension reduction method called diffusion map (DM) (Coifman and Lafon., 2006) is applied to reduce the dimension from p to 2, and then, the degree of closeness of the n ICA components can be visualized by the scatter plot of the two dimensional data. Furthermore, the spectral clustering (Nadler et al., 2006) is used to find the common components across multiple participants in this study.

For group ICA, the temporal concatenation seems to outperform the spatial concatenation (Calhoun et al., 2009). Indeed, this conclusion is based on group ICA for fMRI data mostly in the block or event-related designs. It is unknown whether the conclusion is valid for the fMRI data during real-world experiences. Therefore, both approaches are tried to decompose the fMRI here.

In order to address the issues mentioned above, fMRI data of eleven musicians in a free-listening experiment (Alluri et al., 2012) are used in this study.

2. Method

2.1 Data description

2.1.1 FMRI

Eleven healthy participants (with no neurological, hearing or psy- chological problems) with formal musical training participated in the study (mean age: 23.2 ± 3.7 SD; 5 females). The participants were scanned with fMRI while listening to a stimulus with a rich musical structure, a modern tango Adios Nonino by Astor Piazzolla. The participants were instructed to stay still and to relax while listening to the musical stimulus and to maintain their gaze on the screen. The fMRI measurements were made using a 3-T (3.0T Signa VH/I General Electric) scanner at the Advanced Magnetic Resonance Imaging (AMI) Centre of Aalto University. The duration of the used stimulus was 512 seconds and the sampling frequency of fMRI was 0.5 Hz. A detailed description regarding fMRI data acquisition and preprocessing can be obtained from Alluri et al. (2012). The fMRI data are called conventionally pre-processed data hereinafter.

2.1.2 Musical features

Six musical features representing the perceived Activity, Fullness, Brightness, Timbral Complexity, Key Clarity and Pulse Clarity, were used in this study (Alluri et al., 2012). These acoustic components were derived as a result of principal component analysis performed on 25 acoustic features extracted from the music stimulus. A detailed description of the feature extraction procedure and post-processing of the features can be found in Alluri et al. (2012). The four timbral components are briefly introduced as follows: Activity is associated with roughness and flux of the high end of the spectrum; Fullness, on the other hand, is associated with the presence of spectral fluctuations in lower bands of the spectrum; Brightness is representative of the ratio between energy content in the higher end of the spectrum and lower end of the spectrum; and Timbral Complexity is a measure of the spread and flatness (Wiener

entropy) of the spectrum. The remaining two features represent tonal and rhythmical components, respectively: Key Clarity is the measure of the tonal clarity, and Pulse Clarity is the estimate of the clarity of the pulse (Alluri, et al., 2012).

2.2 Systematic spatial independent component analysis approach

2.2.1 ICA model

ICA has been extensively used to study brain signals (Vigario and Oja., 2008), and it is based on the linear transformation model associating the observations ($\boldsymbol{x}$) and the underlying sources ($\boldsymbol{s}$) in the brain. The model can be expressed as

$$\boldsymbol{x} = \boldsymbol{\mathcal{A}s} + \boldsymbol{n} = \boldsymbol{\mathcal{A}}\mathbf{s}, \tag{1}$$

where, $\boldsymbol{n}$ is senor noise, $\mathbf{s} = \boldsymbol{s} + \boldsymbol{n}$, $\boldsymbol{n} = \boldsymbol{\mathcal{A}n}$, $\boldsymbol{x} = [x_1, x_2, \cdots, x_I]^T$, $\mathbf{s} = \left[s_1, s_2, \cdots, s_J\right]^T$, and $\boldsymbol{\mathcal{A}} \in \boldsymbol{\mathcal{R}}^{I\times J}$ with the full column rank is usually called as the mixing matrix regarding ICA. In spatial ICA for fMRI, each source is indeed the voxel series and can be assembled to a spatial map, and each column of $\boldsymbol{\mathcal{A}}$ denotes the temporal course of the corresponding spatial map. In this study, we assume $I > J$ and this means the number of scans in the fMRI experiment is larger than the number of underlying sources regarding spatial ICA. Hence, the model in Eq. (1) is over-determined. After the number of sources is estimated, the over-determined model can be converted to be determined through

$$\mathbf{x} = \mathbf{V}^{\boldsymbol{T}}\boldsymbol{\mathcal{A}}\mathbf{s} = \mathbf{As}, \tag{2}$$

where $\mathbf{V}^{\boldsymbol{T}} \in \boldsymbol{\mathcal{R}}^{J\times I}$, and $\mathbf{V}^{\boldsymbol{T}}$ is called dimension reduction matrix, $\mathbf{A} \in \boldsymbol{\mathcal{R}}^{J\times J}$, $\mathbf{A} = \mathbf{V}^{\boldsymbol{T}}\boldsymbol{\mathcal{A}}$ and $\mathbf{A}$ is also called the mixing matrix, and $\mathbf{x} = \left[x_1, x_2, \cdots, x_J\right]^T$. The determination of $\mathbf{V}^{\boldsymbol{T}}$ can be based on PCA and model order selection (Li et al., 2007) and this will be discussed later. In order to separate the mixture in Eq. (2), an unmixing matrix is first learned by ICA (Hyvärinen et al., 2001), and then it transforms the mixture in Eq. (2) into independent components as

$$\mathbf{y} = \mathbf{Wx} = \mathbf{WAs} = \mathbf{Cs}, \tag{3}$$

where $\mathbf{W} \in \boldsymbol{\mathcal{R}}^{J\times J}$ is the unmixing matrix, $\mathbf{y} = \left[y_1, y_2, \cdots, y_J\right]^T$ and $\mathbf{y}$ represent the voxel series which can be assembled to spatial maps**.** In order to obtain the temporal course of each spatial map in the original over-determined model, Eq. (1), the inverse of the unmixing matrix is projected to the scan field through the dimension reduction matrix

$$\boldsymbol{\mathcal{U}} = \mathbf{V}\,\mathbf{B} = \mathbf{V}\,\mathbf{W}^{-1}, \tag{4}$$

where, $\mathbf{B} = \mathbf{W}^{-1}$, and $\boldsymbol{\mathcal{U}} \in \boldsymbol{\mathcal{R}}^{I\times J}$ and each of its columns contains the temporal course of corresponding spatial map in $\mathbf{y}$.

For perfect ICA decomposition, there is only one nonzero element in each row and each column of $\mathbf{C}$ in Eq. (3), and y_j the scaled version of s_k (Hyvärinen et al., 2001). It should be noted that the scale is unknown due to the variance indeterminacy of ICA component, and the j in the y_j can be different from the k in the s_k due to the permutation indeterminacy of ICA components (Hyvärinen et al., 2001). Indeed, according to Eq. (1), s_k is not the true source, $\mathcal{s}_k$, but the true source plus decomposed sensor noise, $\mathcal{s}_k + n_k$. If SNR is low, say, less than 0 dB, s_k will be dominated by sensor noise. Although $\mathcal{s}_{j_1}$ is independent with another source $\mathcal{s}_{j_2}$, the independence between s_{j_1} and s_{j_2} will be absolutely weakened since sensor noise is assumed to be Gaussian, which can prevent to obtain satisfactory ICA decomposition.

Therefore, appropriately decreasing additional noise in Eq. (1) can benefit the following ICA decomposition.

2.2.2 Appropriate digital filter to further preprocess fMRI data

In fMRI data, the digital filter can be performed on the temporal course of a voxel (Friston et al., 2000). Regarding the filtering, two fundamental questions are to be answered. The first is how to determine the reasonable pass band of frequencies for the filter, and the second is how to implement the filter with the consideration of the given signal.

The correlation coefficient between the temporal course of a musical feature and the temporal course of a voxel was calculated to determine the region of the interest in the spatial map of fMRI data (Alluri et al., 2012). If the two temporal courses are highly correlated, their spectrum should be similar too. Hence, in this study, we examined the magnitude spectrum of the temporal courses of the musical features to determine the pass band of the digital filter. Fig. 1 presents the temporal course and its magnitude spectrum of each musical feature. It indicates that most of the power of temporal courses is below 100 mHz. Hence, the pass band of the digital filter was set from 8 to 100 mHz in this study. The low cut-off frequency followed the previous pre-processing for this dataset (Alluri et al., 2012).

For fMRI data collection, recordings at the beginning of the experiment are usually not included into analysis since they are much noisier. In this study, the data from 21 to 480 seconds were used for analysis. Hence, the number of scans for analysis is 231 (sampling frequency of the temporal course was 500 mHz, i.e., TR = 2 seconds). We can design the digital filter through Fast Fourier Transform (FFT). For FFT based digital filter, the transformed coefficients out of the pass band are set to be zeros, and then, the modified coefficients series were transformed back to the time-domain to produce the filtered signal.

2.2.3 Estimating number of extracted components

Before ICA, it is necessary to determine how many components to be extracted. For individual ICA, MOS was performed for individual datasets. For the spatial concatenation approach of group ICA, MOS was applied to the grouped data directly. For temporal concatenation approach of group ICA, dimension reduction was firstly done for each participant like that for individual ICA; then, the selected PCA components (each PCA component can be regarded as a virtual scan in fMRI) of different participants were stacked together in the virtual scan space (Calhoun et al., 2009); next, MOS was performed on the stacked data.

For individual datasets, MOS methods including AIC, MDL and KIC based on the resampled fMRI data (Li et al., 2007) and SORTE (He et al., 2010) without the resampling step were applied, and results of MDL and SORTE were used for the individual ICA. For the two grouped datasets, only MDL and SORTE were applied. SORTE was successfully used to estimate the number of sources in EEG data (Cong et al., 2011, 2013). It is very computationally efficient (Cong et al., 2012). Therefore, we tested SORTE for fMRI data here.

2.2.4 ICA decomposition

In this study, ICA was applied on the selected PCA components to extract independent components through software, FastICA (Hyvärinen., 1999) based ICASSO (Himberg et al., 2004). The advantage of this software is that the stability of ICA decomposition is analyzed. It may run one ICA algorithm many times respectively with individually and randomly initialized unmixing matrices; then, all the extracted components are clustered into the predefined number of clusters; finally, each common component in each cluster represents one component extracted by ICASSO (Himberg et al., 2004).

The nonlinear function for FastICA was the hyperbolic tangen, FastICA was run 100 times, and in each round the maximum number of iteration of FastICA was 100 steps. The number of clusters was equal to the number of extracted components. Default parameters in ICASSO were used for the clustering.

The difference of our approach from the default of ICASSO is that the rounds where FastICA did not converge were rejected before the clustering in ICASSO.

2.2.5 Selecting components of interest

After ICA decomposition, each temporal course of each extracted spatial map was correlated with each musical feature. Only the ICA components (i.e., spatial maps) whose temporal courses were significantly correlated with musical features were chosen. After that, if the normalized kurtosis (Hyvärinen et al., 2001) of a selected ICA component (i.e., one spatial map for one participant) was smaller than five, it was rejected in order to remove the scattered spatial maps. Here, 'five' was determined based on empirical experiences. It should be noted that for the group ICA based on the spatial concatenation, one extracted ICA components actually includes all participants' spatial maps, and therefore, it is first disconnected into sub-component for each participant, and each sub-component can be assembled into a spatial map.

For the selected components by ICA, given one musical feature, if the number of participants was equal to or larger than six (more than half of the eleven participants), the selected components were considered to represent information of majority of participants in the experiment, and were further analyzed.

Statistically, it is necessary to investigate the significance of the correlation coefficient between two temporal courses. Then, the threshold to determine the significant correlation coefficient should be given. For such a purpose in this study, one threshold was based on one musical feature and all temporal courses of each participant in individual ICA and group ICA under the temporal concatenation approach. For the spatial concatenation approach of group ICA, there is only one set of temporal courses and they were used to determine the threshold for each musical feature.

Since the temporal courses of spatial maps and musical features are inevitably correlated many times, correction for multiple comparisons should be applied to counter the reduction in statistical power (Groppe et al., 2011). For this purpose, the Monte-Carlo and permutation test procedure presented in (Alluri et al., 2012) were employed to calculate the significance of correlation coefficient and to correct for multiple comparisons. Pearson correlation analysis was applied. The components of interest were then determined as the ones displaying significant correlations ($p < 0.01$) with the musical features.

2.2.6 Clustering selected components

The individual ICA is performed on individual fMRI datasets. Therefore, it is necessary to examine the common information across different participants to draw reliable conclusion (Esposito et al., 2005). Here, we applied diffusion map to reduce the dimension of each selected ICA component, and then, performed the spectral clustering to find the common ICA components across majority of participants (Sipola et al., 2013). For the completeness of the study, diffusion map is introduced as follows.

The initial step of the diffusion map algorithm is to calculate the affinity matrix W, which has data vector distances as its elements. Here Gaussian kernel with Euclidean distance metric is used (Coifman and Lafon., 2006) as below

$$W_{ij} = \exp(-\frac{\|x_i - x_j\|^2}{\epsilon}) \quad (5)$$

where x_i is the p–dimensional data point. The neighborhood size parameter ϵ is determined by finding the linear region in the sum of all weights in W, while trying different values of ϵ (Coifman et al., 2008,Singer et al., 2009).

From the affinity matrix W the row sum diagonal matrix $D_{ii} = \sum_{j=1}^{n} W_{ij}, i \in 1,2,\cdots,n$ is calculated. The W matrix is then normalized as $P = D^{-1}W$. This matrix represents the transition probabilities between the data points, which are the samples for clustering and classification. The conjugate matrix $\tilde{P} = \sqrt{D}P\sqrt{D^{-1}}$ is created in order to find the eigenvalues of P. In practice, substituting P, we obtain

$$\tilde{P} = \sqrt{D^{-1}}W\sqrt{D^{-1}}. \quad (6)$$

This so-called normalized graph Laplacian preserves the eigenvalues (Nadler et al., 2008). Singular value decomposition (SVD) $\tilde{P} = U\Lambda U^*$ yields the eigenvalues $\Lambda = diag([\lambda_1, \lambda_2, \cdots, \lambda_n])$ and eigenvectors in matrix $U = [u_1, u_2, \cdots, u_n]$. The eigenvalues of P and $\tilde{P}$ stay the same. It is now possible to find the eigenvectors of $\tilde{P}$ with $V = \sqrt{D}U$ (Nadler et al., 2008). The low-dimensional coordinates in the embedded space Ψ are created using Λ and Vas

$$\Psi = \Lambda V. \quad (7)$$

Now, for each p–dimensional data point x_i, there is a corresponding d–dimensional coordinate, where $d \ll p$. The number of selected dimensions depends on how fast the eigenvalues decay.

The first few dimensions from the diffusion map represent the data for clustering up to a relative prevision, and thus, contain most of the distance differences in the data (Coifman and Lafon., 2006). Therefore, some of the first dimensions will be used to represent the data. The threshold at 0 in the embedded space divides the space between the possible clusters, which means that a linear classification can be used (Nadler et al., 2006,Meila and Shi., 2000,Shi and Malik., 2000).

In this study, $d = 1$, this means the p–dimensional data were reduced to one dimension for clustering. With the linear threshold, the second eigenvector (the first one is always constant in diffusion map analysis) separates the data into two clusters in the low-dimensional space. This eigenvector solves the normalized cut problem which means that there are small weights between clusters but the internal connections between the members inside the cluster are strong (Meila and Shi., 2000,Shi and Malik., 2000).

3. Result

3.1 Musical features

As show in Fig. 1, Brightness, Fullness, and Activity are similar, and most of their power falls below 100mHz in their spectrum. Moreover, Timbral Complexity keeps the rough trends of those three musical features. Furthermore, Key Clarity is not significantly correlated with any of the other musical features.

3.2 Number of extracted components

3.2.1 Individual ICA

As shown in Fig.2, using any of the information theory based MOS algorithms among AIC, MDL and KIC, the estimated number of sources in the conventionally preprocessed fMRI data (except one subject's result by AIC) was smaller than the estimated number in the further filtered fMRI data by 8-100mHz band pass filter (Hereinafter, when the further filtered fMRI data mentioned, it means the 8-100mHz band

pass filter was used); using SORTE, the numbers of sources in the further filtered fMRI data decreased in contrast to those in the conventionally preprocessed data. For the further filtered fMRI data, AIC, MDL, and KIC gave the identical results. According the previous simulation study (Cong et al., 2012), when SNR is low, the information theory based MOS algorithms tend to underestimate the true number of sources, particularly MDL, and SORTE overestimates it. The results for the real fMRI data here matched the simulation study very well, indicating the SNR in the conventionally preprocessed fMRI data was still too low for MOS.

Furthermore, for the further filtered fMRI data, the estimated number of sources by AIC, MDL and KIC was a little bigger than that by SORTE, which also was observed for the further filtered event-related potentials (ERPs) by performing the wavelet filter on the conventionally preprocessed ERP data (Cong et al., 2013).

Here, for individual ICA on the further filtered fMRI data, 94 components (estimated by SORTE in Fig.2) were extracted. For comparison, individual ICA was also performed on the conventionally preprocessed fMRI data, and the number of extracted components was about 30 (estimated by MDL as shown in Fig.2).

3.2.2 Group ICA

For group ICA, only MDL and SORTE were applied.

For the temporal concatenation, the estimated numbers of sources in the conventionally preprocessed fMRI data were 18 (MDL) and 340 (SORTE), and they were 1 (MDL) and 1012 (SORTE) in the further filtered fMRI data.

For the spatial concatenation, the estimated numbers of sources in the conventionally preprocessed fMRI data were 122 (MDL) and 228 (SORTE), and they were 161 (MDL) and 94 (SORTE) in the further filtered fMRI data.

As a result, for the filtered fMRI data, 94 components (estimated by SORTE) were extracted by group ICA based on the spatial concatenation approach, and group ICA based on the temporal concatenation approach was not applied since the estimated number of components did not seem to be reasonable. For comparison, for the conventionally preprocessed fMRI data, 122 components (estimated by MDL) were extracted by group ICA based on the spatial concatenation approach, and 18 components (estimated by MDL) were extracted by group ICA based on the temporal concatenation approach.

3.3 Selected components regarding musical features

3.3.1 Individual ICA

3.3.1.1 Further filtered fMRI data

Fig.3-a shows the similarity matrix of the selected components whose temporal courses were significantly correlated with one musical feature. Among the six musical features, four of them were chosen since the number of participants (possessing components whose temporal courses were significantly correlated with one musical feature) was larger than half of all eleven participants regarding each of the four ones.

After the components of interest were selected, the common component across the majority of participants was found via diffusion map and spectral clustering. Fig.3-b shows the spectral clustering results for the components regarding Brightness. Here, ten components from ten participants were found to formulate one dense group. Those ten components actually correspond to the ten components showing higher correlation coefficients in the similarity matrix for Brightness in Fig.3-a. Indeed, as long as the threshold of the correlation coefficient was correctly defined, the common component could also be found

based on the similarity matrix of the selected components. However, defining the threshold tends to be challenging and subjective. Based on the diffusion map, the spectral clustering can easily group the data points by using the objective threshold '0' as mentioned in the previous section.

Fig.3-c shows the spatial map of the average over the ten components in the dense group. Obviously, the auditory cortex was activated. Before averaging, each component was normalized to its standard deviation and subtracted its means.

For Activity, seven components from seven participants were clustered into a dense group. They were actually included into the ten components mentioned above. For Fullness and Timbral Complexity there were no more than five participants showing similar components.

As a result, by the individual ICA on the further filtered fMRI data, two musical features, Brightness and Activity, were found to be significantly correlated with the fMRI data of majority of participants. The selected common spatial maps regarding each of the two features were further analyzed.

3.3.1.2 ROI analysis

We performed region of interest (ROI) analysis on the spatial maps for Brightness and Activity, which had been averaged from common components across more than 50% of participants. The results show highly significant areas mainly within and surrounding the auditory cortices. A slight right-lateralized effect was observed in both maps. For both the two selected musical features, one large cluster at each hemisphere was identified (see Table 2 for a list of the clusters). The bilateral superior temporal gyrus (STG) was the most sizable region across both maps (k>1100), followed by the left middle temporal gyrus (MTG; k>550). Other common areas across both maps were the bilateral rolandic operculum (k>55) and bilateral Heschl's gyrus (k>65), both predominantly right-lateralized, plus the right insula (k>24). Similarly, the temporal pole of the STG (k>77) showed a rightward bias, whereas the supramarginal gyrus (SMG; k>11) displayed dissimilar hemispheric weightings in both maps.

3.3.1.3 Conventionally preprocessed fMRI data

Fig.4 shows the similarity matrix of the selected components whose temporal courses were significantly correlated with one musical feature. Among six musical features, only three of them were chosen since the number of participants (possessing components whose temporal courses were significantly correlated with one musical feature) was larger than half of all eleven participants regarding each of the three ones.

However, for any of the selected three features, there were no more than five participants showing common components.

3.3.2 Group ICA

3.3.2.1 Further filtered fMRI data

Temporal concatenation approach was not applied since the estimated number of components did not seem reasonable.

By the spatial concatenation approach, only one ICA component was selected since just this corresponding temporal course was significantly correlated with the musical feature (Brightness here) and the number of selected participants was larger than half of all eleven participants. Here, eight out of eleven participants were selected since the normalized kurtoses of their spatial maps were all larger than five. For the other five musical features, no components satisfied those conditions.

3.3.2.2 Conventionally preprocessed fMRI data

Temporal concatenation approach was applied. However, there was no component whose temporal courses of more than half of all eleven participants were simultaneously correlated with any musical feature significantly.

By the spatial concatenation approach, only one ICA component was selected since just this corresponding temporal course was significantly correlated with the musical feature (Brightness here) and the number of selected participants was larger than half of all eleven participants. Here, nine out of eleven participants were selected since the normalized kurtoses of their spatial maps were all larger than five. For other five musical features, no components satisfied those conditions.

All the eight spatial maps used for Figs.5&6 showed the auditory cortex activated like the spatial map in Fig.3-c. For simplicity of the study, the spatial maps used for Figs.5&6 are not presented here.

3.4 Kurtoses of selected components regarding musical features

Table-1 gives the mean, standard deviation, minimum, median and maximum of the kurtoses of the finally selected spatial maps (e.g., ICA components) regarding each selected musical feature for each method. The kurtosis was used to select the component of interest here. Obviously, the spatial maps extracted by individual ICA from the further filtered fMRI data are much more super-Gaussian than those by any other methods.

Discussion

ICA has been often used to process fMRI data nowadays mostly for the resting-state, block and event-related designs due to its outstanding advantage (Calhoun et al., 2009,Calhoun and Adali., 2012). For the fMRI data during real-world experiences, only a few studies reported the application of ICA (Malinen et al., 2007,Ylipaavalniemi et al., 2009). In the present study, key issues in applying ICA on fMRI data during free-listening to naturalistic and continuous music were investigated.

First of all, different from most of studies using ICA to decompose fMRI data, a digital filter was further performed on the temporal course of each voxel after the conventionally pre-processing step in order to further remove sources of no interest and noise before ICA. In this study, the pass band of the FFT based digital filter was set to 8-100 mHz, which can be regarded as the combination of a high pass filter with the cut-off frequency at 8 mHz and a low pass filter with the cut-off frequency at 100 mHz. The low cut-off frequency has been used in the conventional pre-processing step to remove the low-frequency drift artifacts (Alluri et al., 2012). The determination of the high cut-off frequency was based on the magnitude spectrum of the musical features of the auditory stimulus since the selection of ICA components of interest is based on the correlation between the temporal courses of musical features and the temporal courses of the ICA components. Furthermore, the sampling frequency is 500 mHz and the folding frequency is 250 mHz here. Given such a sampling frequency, if the highest frequency in the signal to be recorded is no greater than 250 mHz, all the frequency components can be recovered according to the well-known sampling theorem. However, it is difficult to determine that the highest frequency component in fMRI data is not over 250 mHz, and the possibly existing frequency components which are higher than 250 mHz can appear as artifactual low frequencies in the digitized data (Luck, 2005). Moreover, each digital filter practically cannot avoid the transitional band. Therefore, the high cut-off frequency is essential to be lower than the folding frequency. In practice, the high cut-off frequency should be no more than one third of the sampling frequency (Luck, 2005).

Secondly, for individual ICA, the estimation by model order selection methods on the conventionally pre-processed fMRI data and the further filtered fMRI data indicated that the estimated number of sources in the former data seemed not to be precise, but tended to be reasonable in the latter data as shown in 3.2.1. Indeed, when SNR is low, it is very difficult to accurately estimate the model

order (Cong et al., 2012). Therefore, it is expected that the FFT filter used in this study could benefit the model order selection. Particularly, the fast model order selection method, the eigenvalues' gap based SORTE (He et al., 2010), worked very well for the further filtered fMRI data. It is very promising to use the gap based method for model order selection (Cong et al., 2012) when ICA is applied for the fMRI data processing.

Thirdly, individual ICA on the filtered fMRI data outperformed individual ICA on the conventionally pre-processed fMRI data from the point of view of the degree of the correlation between the fMRI data of majority participants and the musical features of the music stimulus. We think the main reason origins from the number of extracted components, i.e., the estimated number of sources. For the conventionally pre-processed fMRI data, the number of extracted components was about 30 by MDL in this study, and this number seemed to be much smaller than the true number of sources in the data with the reference to the estimated number of sources from the further filtered fMRI data. Therefore, selecting 30 PCA components of the conventionally pre-processed fMRI data for ICA made the linear transform model of the selected data undetermined, i.e., the true number of sources is larger than the number of observed signals (e.g., the number of selected PCA components here). It is not surprising that the results could be worse when the determined ICA algorithm was applied on the underdetermined mixtures.

Fourthly, based on the spatial concatenation approach, group ICA on the filtered fMRI data did not significantly differentiate from group ICA on the conventionally pre-processed fMRI data. Furthermore, the spatial concatenation based group ICA outperformed the temporal concatenation based group ICA from the point of view of the estimation of number of sources and the degree of the correlation between the fMRI data of majority participants and the musical features.

Fifthly, using individual ICA from the further pre-processed fMRI data, we found two musical features (Brightness and Activity) were significantly correlated with the temporal courses of the common spatial maps of majority of participants. For group ICA on the further filtered fMRI data or the conventionally pre-processed fMRI data, only one musical feature (Brightness) was found. Furthermore, by the individual ICA, there were more components whose temporal courses were significantly correlated with the musical features, and those components which were not common across majority of participants were difficult for group ICA to extract out. Moreover, it has been recently again proved that ICA is indeed based on independence among non-Gaussian sources (Calhoun et al., 2013). From this point of view, the individual ICA on the further filtered fMRI data outperformed any other methods in this study since the selected ICA components by this method were the most super-Gaussian. However, group ICA is much more straightforward for the group-level comparison than the individual ICA (Calhoun et al, 2009). The similar results between individual ICA and group ICA here guarantee the rationale in using group ICA for the fMRI data during real-world experiences in the future.

Sixthly, finding common spatial maps across different participants was based on the diffusion map dimensionality reduction (Coifman and Lafon, 2006) and spectral clustering (Nadler et al., 2006) in this study. The approach was earlier compared to other clustering methods, namely PCA and kernel PCA based spectral clustering, and hierarchical clustering based on the similarity matrix. For details, please refer to our previous study (Sipola et al., 2013). Diffusion map reduces dimensionality of the data from hundreds of thousands to two for easier clustering. The reduced data conveniently visualizes the distribution of data samples in the two-dimensional space. The assumption that most of the spatial maps describing a response to a certain stimulus are similar leads to the belief that they form clusters. Diffusion map finds a structure based on the transition probabilities between samples. The obtained clustering is meaningful in that sense, finding a description of the data that separates the clusters.

Finally, our study is different from Malinen et al. (2007) and Ylipaavalniemi et al. (2009) in selecting the interesting spatial maps extracted by ICA from fMRI data elicited by the naturalistic stimulus. In Malinen et al. (2007), the spatial maps of interest were chosen based on roughly inspecting

the correlations between the stimulus sequence and the temporal courses of the corresponding spatial maps. In Ylipaavalniemi et al. (2009), they were decided according to the canonical correlation analysis (CCA) between the temporal courses of acoustical features of speech and those of spatial maps. Our study examined the statistically significant correlation coefficients between the temporal course of each musical feature and those of spatial maps since we wanted to examine each musical feature individually. Furthermore, since the significance of the correlation coefficient was determined by the Monte-Carlo and permutation test procedure, the condition to select a spatial map of interest was stricter here.

The results derived from the common spatial maps per feature obtained from our individual ICA approach and further clustering method intersect with those obtained by Alluri et al. (2012) using the same set of musical features and fMRI data acquired during a continuous, free listening condition. Thus, the map of relevant regions for Activity was virtually identical to the one found by the preceding authors, comprising most of the two largest clusters recruited in their study, with very similar regional contributions. Other cerebellar correlates observed in their study were not identified, nor were common negative correlating regions in the frontal and parietal lobes across most of the participants observed. For Brightness our results closely resemble the largest foci in Alluri et al. (2012) at each hemisphere. Similarly as with Activity, our method failed to map the areas outside these two large auditory cortical clusters, i.e., in the basal ganglia and cerebellum.

Overall, we observed agreement with the results reported in Alluri et al. (2012). More specifically, the present ICA approach seemed to be sensitive to the largest clusters present in the aforementioned study pertaining to the auditory cortical surface, and rather insensitive in detecting smaller clusters in other cerebral and cerebellar areas.

Acknowledgement

This work was supported by TEKES (Finland) grant 40334/10 ‘Machine Learning for Future Music and Learning Technologies’. Asoke K Nandi would like to thank TEKES for their award of the Finland Distinguished Professorship. Tuomo Sipola’s work was partially supported by the Foundation of Nokia Corporation. Authors thank GIFT software (http://mialab.mrn.org/software/gift/) for model order selection and group ICA.

References

Akaike H. A new look at statistical model identification. IEEE Trans. Autom. Control, 1974;19:716-23.

Alluri V, Toiviainen P, Jaaskelainen IP, Glerean E, Sams M, Brattico E. Large-scale brain networks emerge from dynamic processing of musical timbre, key and rhythm. Neuroimage, 2012;59:3677-89.

Calhoun VD, Adali T. Multisubject independent component analysis of fMRI: a decade of intrinsic networks, default mode, and neurodiagnostic discovery. IEEE Rev.Biomed.Eng., 2012;5:60-73.

Calhoun VD, Adali T, Pearlson GD, Pekar JJ. Spatial and temporal independent component analysis of functional MRI data containing a pair of task-related waveforms. Hum.Brain Mapp., 2001;13:43-53.

Calhoun VD, Liu J, Adali T. A review of group ICA for fMRI data and ICA for joint inference of imaging, genetic, and ERP data. Neuroimage, 2009;45:S163-72.

Calhoun VD, Potluru VK, Phlypo R, Silva RF, Pearlmutter BA, Caprihan A, Plis SM, Adali T. Independent component analysis for brain fMRI does indeed select for maximal independence, PLoS One 2013 (Accepted for publication)

Cavanaugh JE. A large-sample model selection criterion based on Kullback's symmetric divergence. Stat. Probab. Lett., 1999;44:333-44.

Coifman RR, Lafon S. Diffusion maps. Appl. Comput. Harmon. Anal., 2006;21:5-30.

Coifman RR, Shkolnisky Y, Sigworth FJ, Singer A. Graph Laplacian tomography from unknown random projections. IEEE Trans.Image Process., 2008;17:1891-9.

Cong F, He Z, Hämäläinen J, Leppänen PHT, Lyytinen H, Cichocki A, Ristaniemi T. Validating Rationale of Group-level Component Analysis based on Estimating Number of Sources in EEG through Model Order Selection. Journal of Neuroscience Methods, 2013;212:165-72.

Cong F, He Z, Hämäläinen J, Cichocki A,Ristaniemi T. Determining the Number of Sources in High-density EEG Recordings of Event-related Potentials by Model Order Selection. Proc IEEE MLSP2011:1-6.

Cong F, Nandi AK, He Z, Cichocki A, Ristaniemi T. Fast and Effective Model Order Selection Method to Determine the Number of Sources in a Linear Transformation Model. Proc. The 2012 European Signal Processing Conference (EUSIPCO-2012), 2012:1870-4.

Erhardt EB, Rachakonda S, Bedrick EJ, Allen EA, Adali T, Calhoun VD. Comparison of multi-subject ICA methods for analysis of fMRI data. Hum.Brain Mapp., 2010.

Esposito F, Scarabino T, Hyvarinen A, Himberg J, Formisano E, Comani S, Tedeschi G, Goebel R, Seifritz E, Di Salle F. Independent component analysis of fMRI group studies by self-organizing clustering. Neuroimage, 2005;25:193-205.

Friston KJ, Josephs O, Zarahn E, Holmes AP, Rouquette S, Poline J. To smooth or not to smooth? Bias and efficiency in fMRI time-series analysis. Neuroimage, 2000;12:196-208.

Groppe DM, Urbach TP, Kutas M. Mass univariate analysis of event-related brain potentials/fields I: a critical tutorial review. Psychophysiology, 2011;48:1711-25.

Hasson U, Nir Y, Levy I, Fuhrmann G, Malach R. Intersubject synchronization of cortical activity during natural vision. Science, 2004;303:1634-40.

Haynes JD, Rees G. Decoding mental states from brain activity in humans. Nat.Rev.Neurosci., 2006;7:523-34.

He Z, Cichocki A, Xie S, Choi K. Detecting the number of clusters in n-way probabilistic clustering. IEEE Trans.Pattern Anal.Mach.Intell., 2010;32:2006-21.

Hickok G, Buchsbaum B, Humphries C, Muftuler T. Auditory-motor interaction revealed by fMRI: speech, music, and working memory in area Spt. J.Cogn.Neurosci., 2003;15:673-82.

Himberg J, Hyvärinen A, Esposito F. Validating the independent components of neuroimaging time series via clustering and visualization. Neuroimage, 2004;22:1214-22.

Hu D, Yan L, Liu Y, Zhou Z, Friston KJ, Tan C, Wu D. Unified SPM-ICA for fMRI analysis. Neuroimage, 2005;25:746-55.

Hyvärinen A. Fast and robust fixed-point algorithms for independent component analysis. IEEE Trans.Neural Netw., 1999;10:626-34.

Hyvärinen A, Karhunen J, Oja E. Independent Component Analysis, John Wile & Sons Inc.: New York, 2001.

Kauppi JP, Jaaskelainen IP, Sams M, Tohka J. Inter-subject correlation of brain hemodynamic responses during watching a movie: localization in space and frequency. Front.Neuroinform, 2010;4.

Kay KN, Naselaris T, Prenger RJ, Gallant JL. Identifying natural images from human brain activity. Nature, 2008;452:352-5.

Koelsch S. Towards a neural basis of music-evoked emotions. Trends Cogn.Sci., 2010;14:131-7.

Koelsch S, Fritz T, Schulze K, Alsop D, Schlaug G. Adults and children processing music: an fMRI study. Neuroimage, 2005;25:1068-76.

Lee K, Tak S, Ye JC. A data-driven sparse GLM for fMRI analysis using sparse dictionary learning with MDL criterion. IEEE Trans.Med.Imaging, 2010.

Li YO, Adali T, Calhoun VD. Estimating the number of independent components for functional magnetic resonance imaging data. Hum.Brain Mapp., 2007;28:1251-66.

Luck SJ, (2005) An Introduction to the Event-Related Potential Technique. The MIT Press. Page-177.

Malinen S, Hlushchuk Y, Hari R. Towards natural stimulation in fMRI--issues of data analysis. Neuroimage, 2007;35:131-9.

McKeown MJ, Makeig S, Brown GG, Jung TP, Kindermann SS, Bell AJ, Sejnowski TJ. Analysis of fMRI data by blind separation into independent spatial components. Hum.Brain Mapp., 1998;6:160-88.

Meila M, Shi JB. Learning segmentation by random walks. Proc. NIPS2000, 2000:873-9.

Nadler B, Lafon S, Coifman RR, Kevrekidis IG. Diffusion maps—a probabilistic interpretation for spectral embedding and clustering algorithms. Lecture Notes in Computational Science and Engineering, 2008;58:238-60.

Nadler B, Lafon S, Coifman RR, Kevrekidis IG. Diffusion maps, spectral clustering and reaction coordinates of dynamical systems. Appl. Comput. Harmon. Anal., 2006;21:113-27.

Pan H, Epstein J, Silbersweig DA, Stern E. New and Emerging Imaging Techniques for Mapping Brain Circuitry. Brain Res.Rev., 2011;67:226-51.

Price CJ. The anatomy of language: a review of 100 fMRI studies published in 2009. Ann.N.Y.Acad.Sci., 2010;1191:62-88.

Rissanen J. Modeling by the shortest data description. Automatica, 1978;14:465-71.

Shi JB, Malik L. Normalized cuts and image segmentation. IEEE Trans. Pattern Anal. Mach. Intell., 2000;22:888-905.

Singer A, Erban R, Kevrekidis IG, Coifman RR. Detecting intrinsic slow variables in stochastic dynamical systems by anisotropic diffusion maps. Proc.Natl.Acad.Sci.U.S.A., 2009;106:16090-5.

Sipola T, Cong F, Ristaniemi T, Alluri V, Toiviainen P, Brattico E, Nandi AK. Diffusion Map for Clustering FMRI Spatial Maps Extracted by Independent Component Analysis. Accepted for publication in IEEE MLSP2013 (http://arxiv.org/abs/1306.1350), 2013.

Spiers HJ, Maguire EA. Decoding human brain activity during real-world experiences. Trends Cogn.Sci., 2007;11:356-65.

Tootell RB, Hadjikhani NK, Mendola JD, Marrett S, Dale AM. From retinotopy to recognition: fMRI in human visual cortex. Trends Cogn.Sci., 1998;2:174-83.

Tzourio-Mazoyer N, Landeau B, Papathanassiou D, Crivello F, Etard O, Delcroix N, Mazoyer B, Joliot M (2002). Automated anatomical labeling of activations in SPM using a macroscopic anatomical parcellation of the MNI MRI single-subject brain. Neuroimage, 15, 273-89.

Vigario R, Oja E. BSS and ICA in Neuroinformatics: From Current Practices to Open Challenges. IEEE Reviews in Biomedical Engineering, 2008;1:50-61.

Ylipaavalniemi J, Savia E, Malinen S, Hari R, Vigario R, Kaski S. Dependencies between stimuli and spatially independent fMRI sources: towards brain correlates of natural stimuli. Neuroimage, 2009;48:176-85.

Table

Table-1: Normalized kurtoses of selected ICA components for each method regarding each selected musical feature: ICA-1 is individual ICA on the further filtered fMRI data, ICA-2 is individual ICA on the conventionally pre-processed fMRI data, ICA-3 is group ICA on the further filtered fMRI data, and ICA-4 is group ICA on the conventionally pre-processed fMRI data.

Method | Parameter	Number of selected components: R	Mean of R kurtoses	Standard deviation of R kurtoses	Minimum of R kurtoses	Median of R kurtoses	Maximum of R kurtoses
ICA-1: Fullness	9	35.8	23.7	9.8	28.1	78.5
ICA-1: Brightness	17	35.6	18.8	9.6	35.3	68.9
ICA-1: Timbral Complexity	6	21.4	13.6	8.1	16.4	40.9
ICA-1: Activity	15	37.3	20.5	9.8	35.3	78.5
ICA-2: Fullness	7	16.2	13.3	6.2	11.7	44.7
ICA-2: Brightness	10	23.5	16.5	7.2	20.1	55.5
ICA-2: Activity	8	21.9	10.5	11.7	19.8	44.7
ICA-3: Brightness	8	12.7	6.7	5.2	12.7	23.0
ICA-4: Brightness	9	12.5	7.3	5.3	12.9	29.1

Table-2: Results of the region on interest (ROI) analysis using Marsbar v0.43[1] on the clusters obtained via the 18-connectivity scheme employed in SPM. Clusters were extracted from the averaged spatial maps across more than 50% of participants (for Activity and Brightness). The significance threshold was set to p=.001 (Z=3.29), and regions ≤ 10 voxels were rejected. The table reports hemispheric location, within-cluster region size (k; i.e., number of voxels), the peak Z-score per region within the cluster, and its respective MNI coordinates. Anatomical areas within the clusters were determined using Automated Anatomical Labeling (AAL; Tzourio-Mazoyer et al., 2002). Abbreviations: STM (superior temporal gyrus), MTG (middle temporal gyrus), SMG (supramarginal gyrus)

LEFT	k	max Z	x	y	z	RIGHT	k	max Z	x	y	z
ACTIVITY											
Cluster #1						Cluster #2					
STG	1161	13.89	-58	-10	2	STG	1474	13.01	62	-16	8
MTG	571	9.99	-56	-16	0	Rolandic operculum	208	10.53	56	-16	10
Heschl's gyrus	65	8.64	-54	-16	8	Heschl's gyrus	199	11.47	58	-10	6
Rolandic operculum	55	6.27	-46	-30	14	Temporal pole, STG	85	7.56	56	4	-4
SMG	15	5.51	-54	-26	14	Insula	24	8.32	50	-4	0
						SMG	13	3.83	56	-36	24
						Postcentral gyrus	11	6.11	64	-16	14
BRIGHTNESS											
Cluster #1						Cluster #2					
STG	1183	13.88	-58	-10	2	STG	1499	12.83	60	-14	6
MTG	556	9.93	-56	-16	0	Heschl's gyrus	211	12.01	54	-10	4
Heschl's gyrus	83	8.16	-54	-16	8	Rolandic operculum	164	9.43	56	-16	10
Rolandic operculum	60	5.89	-46	-30	14	Temporal pole, STG	77	6.50	58	2	0
SMG	11	5.01	-64	-24	14	Insula	34	8.39	50	-4	0

[1] MarsBaR v0.43 (http://marsbar.sourceforge.net)

Figure

Figure 1: a) Temporal courses of six musical features, b) Magnitude spectrums of six musical features

Figure 2: Estimated number of sources for individual ICA

Figure 3: Results of individual ICA on the further filtered fMRI data: a) Similarity matrix of selected components regarding each selected musical feature (the title of each subplot shows the name of the selected musical feature), b) Demo for diffusion map based spectral clustering, c) Spatial map

Figure 4: Results of individual ICA on the conventionally preprocessed fMRI data: Similarity matrix of selected components regarding each selected musical feature. The title of each subplot shows the name of the selected musical feature.

Figure 5: Results of group ICA on the further preprocessed fMRI data: Similarity matrix of selected components. The title of the figure shows the name of the selected musical feature,

Figure 6: Results of group ICA on the conventionally preprocessed fMRI data: Similarity matrix of selected components. . The title of the figure shows the name of the selected musical feature,

Fig. 1-a

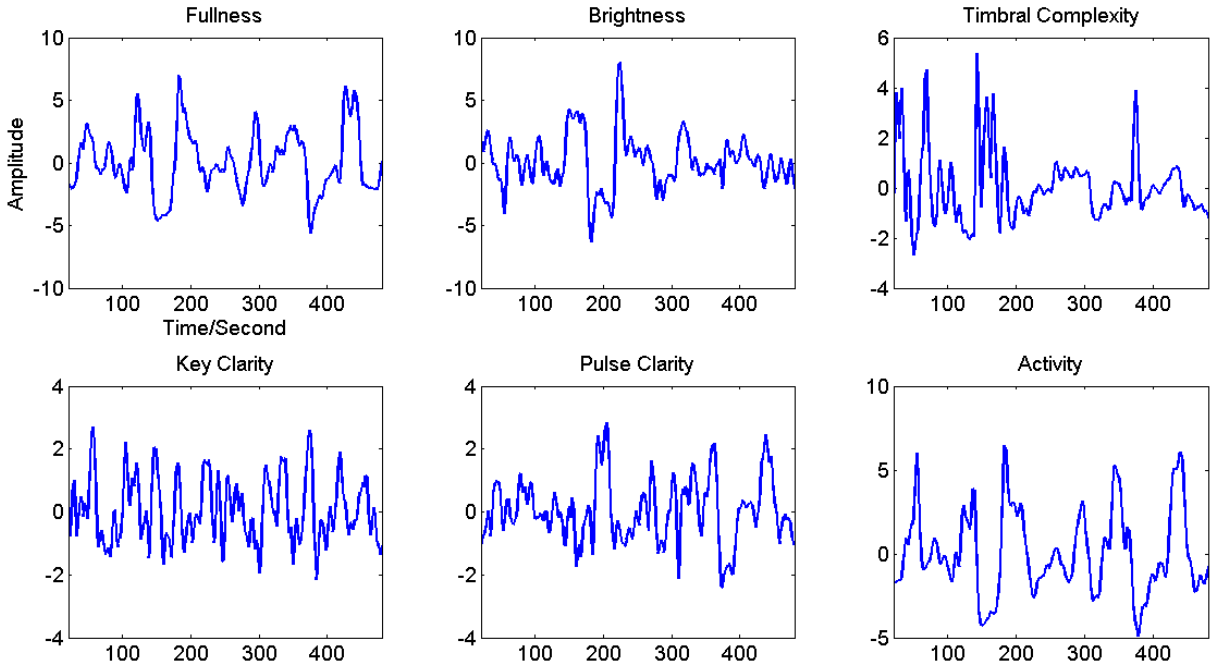

Fig. 1-b

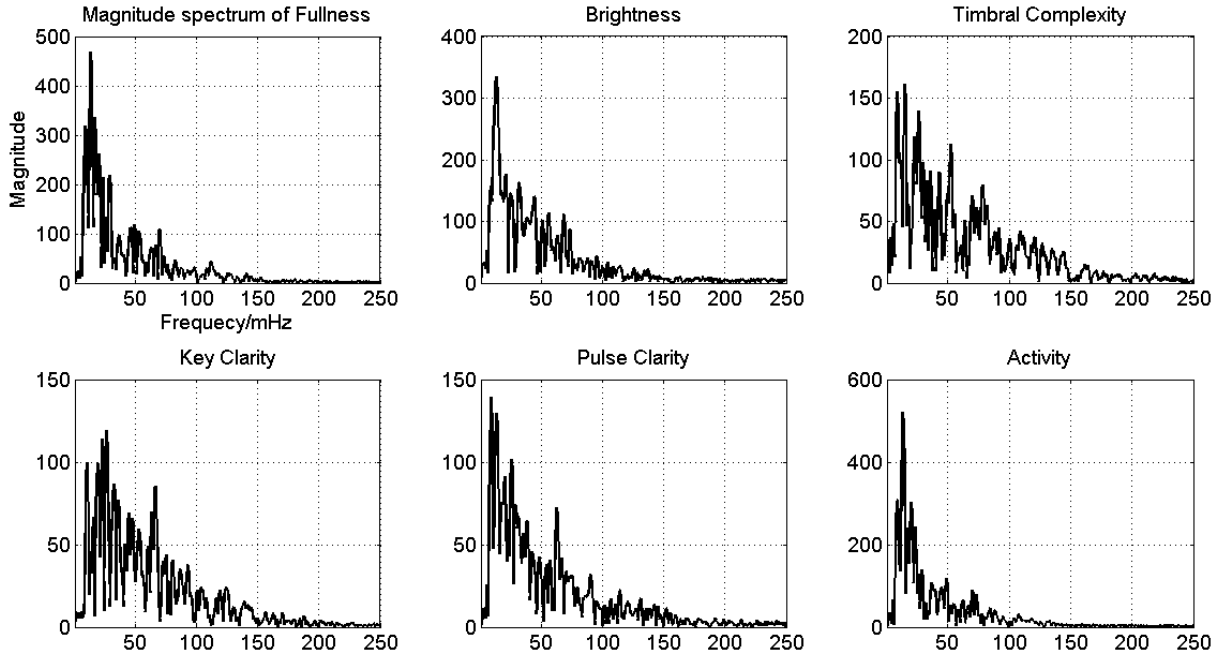

Fig. 2

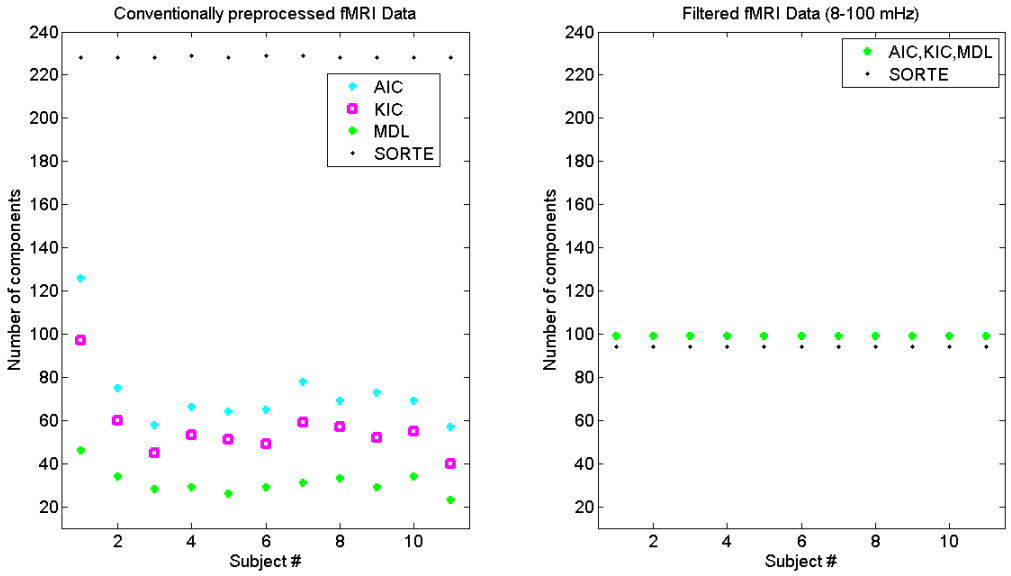

Fig. 3-a

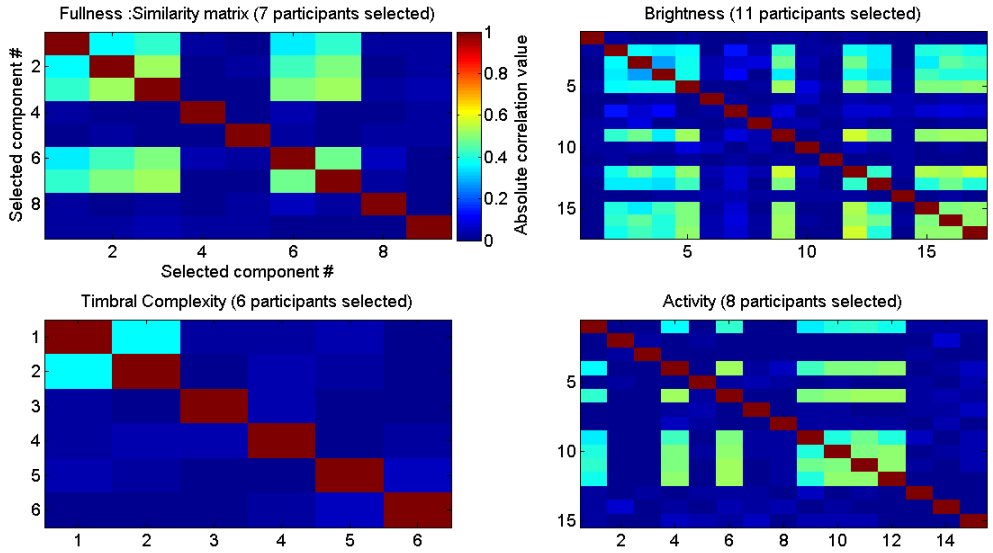

Fig. 3-b

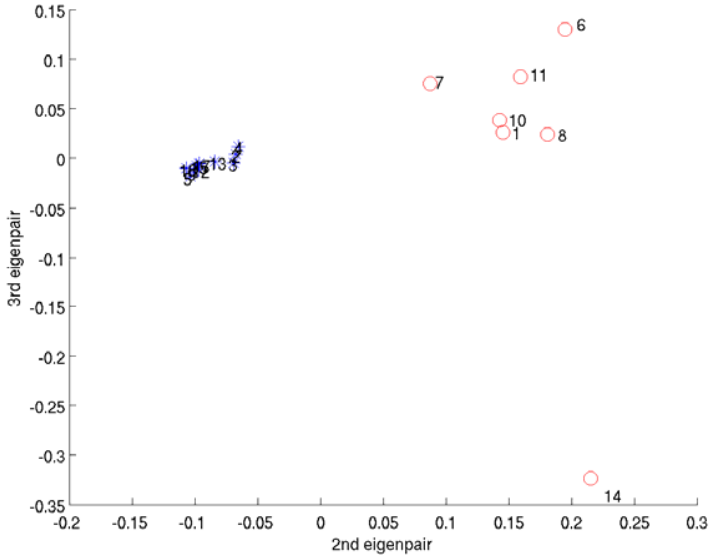

Fig. 3-c

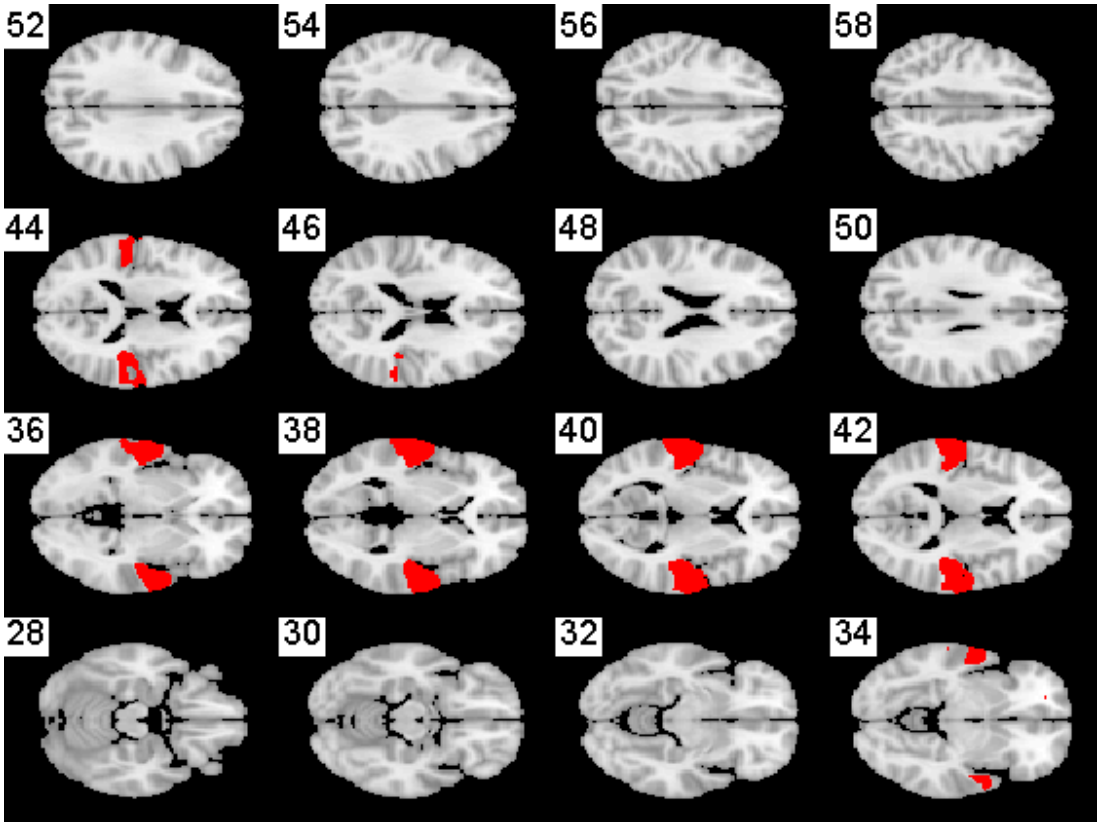

Fig. 4

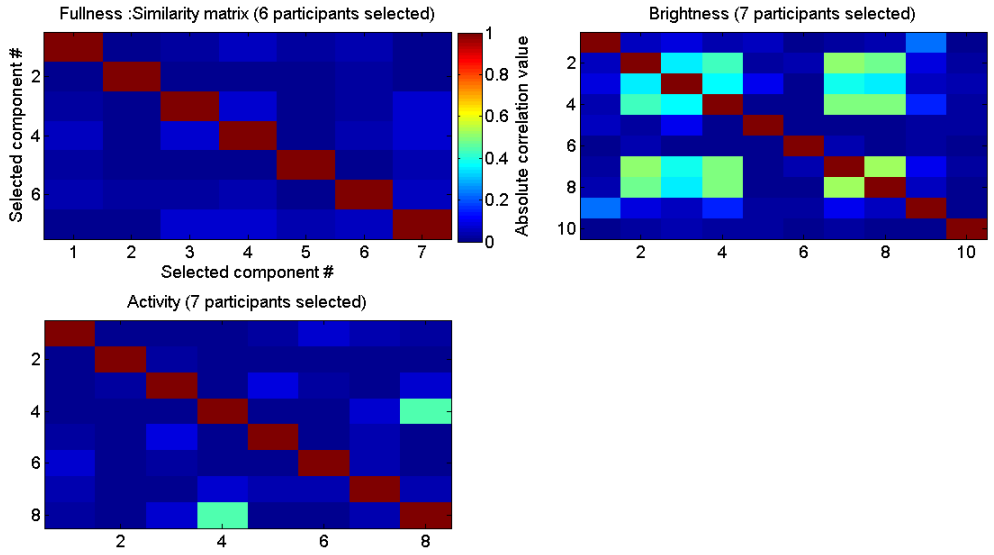

Fig. 5

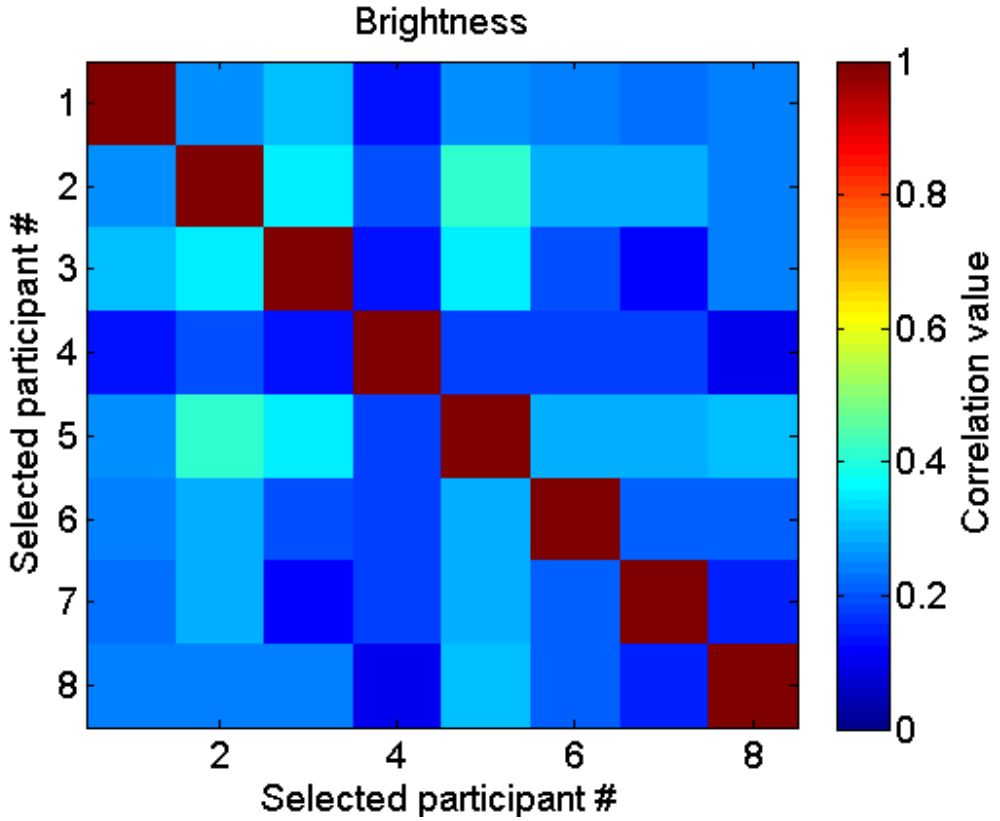

Fig. 6